In Vivo Myoblasts Tracking Using the Sodium Iodide Symporter Gene Expression in Dogs

Isabel Punzón, David Mauduit, Bryan Holvoet, Jean-Laurent Thibaud, Pauline de Fornel, Christophe Deroose, Nicolas Blanchard-Gutton, Jean-Thomas Vilquin, Maurilio Sampaolesi, Inès Barthélémy, et al.

Molecular Therapy
Methods & Clinical Development
Original Article

In Vivo Myoblasts Tracking Using the Sodium Iodide Symporter Gene Expression in Dogs

Isabel Punzón,[1] David Mauduit,[1] Bryan Holvoet,[2] Jean-Laurent Thibaud,[3] Pauline de Fornel,[3] Christophe M. Deroose,[2] Nicolas Blanchard-Gutton,[1] Jean-Thomas Vilquin,[4] Maurilio Sampaolesi,[5] Inès Barthélémy,[1] and Stéphane Blot[1]

[1]INSERM U955-E10, IMRB, Université Paris Est Créteil, Ecole nationale vétérinaire d'Alfort, 94700 Maisons-Alfort, France; [2]Nuclear Medicine and Molecular Imaging, Department of Imaging and Pathology, KU Leuven, Leuven 3000, Belgium; [3]MICEN Vet Clinic, 94000 Créteil, France; [4]Sorbonne Université, INSERM, AIM, Centre de Recherche en Myologie, UMRS 974, AP-HP, Hôpital Pitié Salpêtrière, 75013 Paris, France; [5]Translational Cardiomyology Laboratory, Stem Cell and Developmental Biology, Department of Development and Regeneration, KU Leuven, Leuven, Belgium

Stem cell-based therapies are a promising approach for the treatment of degenerative muscular diseases; however, clinical trials have shown inconclusive and even disappointing results so far. Noninvasive cell monitoring by medicine imaging could improve the understanding of the survival and biodistribution of cells following injection. In this study, we assessed the canine sodium iodide symporter (cNIS) reporter gene as an imaging tool to track by single-photon emission computed tomography (SPECT/CT) transduced canine myoblasts after intramuscular (IM) administrations in dogs. cNIS-expressing cells kept their myogenic capacities and showed strong $^{99\ m}$Tc-pertechnetate ($^{99\ m}TcO_4^-$) uptake efficiency both *in vitro* and *in vivo*. cNIS expression allowed visualization of cells by SPECT/CT along time: 4 h, 48 h, 7 days, and 30 days after IM injection; biopsies collected 30 days post administration showed myofiber's membranes expressing cNIS. This study demonstrates that NIS can be used as a reporter to track cells *in vivo* in the skeletal muscle of large animals. Our results set a proof of concept of the benefits NIS-tracking tool may bring to the already challenging cell-based therapies arena in myopathies and pave the way to a more efficient translation to the clinical setting from more accurate pre-clinical results.

INTRODUCTION

Cell therapy for degenerative skeletal muscle diseases is a promising therapeutic approach;[1,2] however, biodistribution and long-term survival of the administered therapeutic cells are still challenging topics, being both critical factors that may have an impact on the efficacy but also on the safety of this promising therapeutic approach. Duchenne muscular dystrophy (DMD) is an X-linked genetic disease caused by a mutation in the dystrophin gene that results in the absence of the protein[3] leading to progressive muscle wasting.[4] All body muscles progressively degenerate as they are submitted to cycles of regeneration-degeneration that ultimately lead to adipose and fibrotic tissue accumulation.[5] Affected boys present muscle weakness with first walking disabilities in the teens and respiratory and cardiac failures leading to premature death in the third-fourth decades.[6] There is no cure to date for this disease, but research in gene and cell-based therapies has shown encouraging results.[7–9] The discovery of new cell types displaying myogenic properties such as mesoangioblasts (MABs), muscle-derived stem cells, MuStem, and pluripotent cells committed to myogenic fates gave new hopes for cell-based therapies.[10–12] The choice of an adequate therapeutic cell is a critical factor when it comes to ensure cell-based therapies' success; however, discussions on the most relevant characteristics these cells must fulfill are still ongoing and no agreement across the community has been reached yet.[13]

Selection of the appropriate relevant animal model is a critical point for validating preclinical data. In the case of DMD, the model of choice that best resembles the physiopathology and clinical evolution process is the golden retriever muscular dystrophy dog (GRMD).[14] With this model, we have demonstrated the efficiency of MABs in dystrophin restoration and functional improvement.[15] However, until now, preclinical studies in large animal models were hampered by the lack of methodologies allowing adequate non-invasive assessment of the biodistribution pattern and survival rate of transplanted cells. These two parameters are key elements for the treatment of chronic skeletal muscle wastage. More accurate information on therapeutic transplanted cell's fate is needed for a better translation from preclinical models to clinical trials, which have so far only shown inconclusive results.[16] Methodological developments should be aimed at providing insight on key questions such as the optimum therapeutic cell dose, route of administration, cell migration patterns, potential risk of cell transformation, inflammatory events, and/or non-desired immune reactions.

Sodium iodide symporter (NIS) gene-expression system may help address some of the aforementioned critical questions. NIS allows

Received 7 July 2019; accepted 13 December 2019;
https://doi.org/10.1016/j.omtm.2019.12.011.

Correspondence: Isabel Punzón, PhD, INSERM U955-E10, IMRB, Université Paris Est Créteil, Ecole nationale vétérinaire d'Alfort, 94700 Maisons-Alfort, France.
E-mail: isabel.punzon@vet-alfort.fr
Correspondence: Stéphane Blot, INSERM U955-E10, IMRB, Université Paris Est Créteil, Ecole nationale vétérinaire d'Alfort, 94700 Maisons-Alfort, France.
E-mail: stephane.blot@vet-alfort.fr

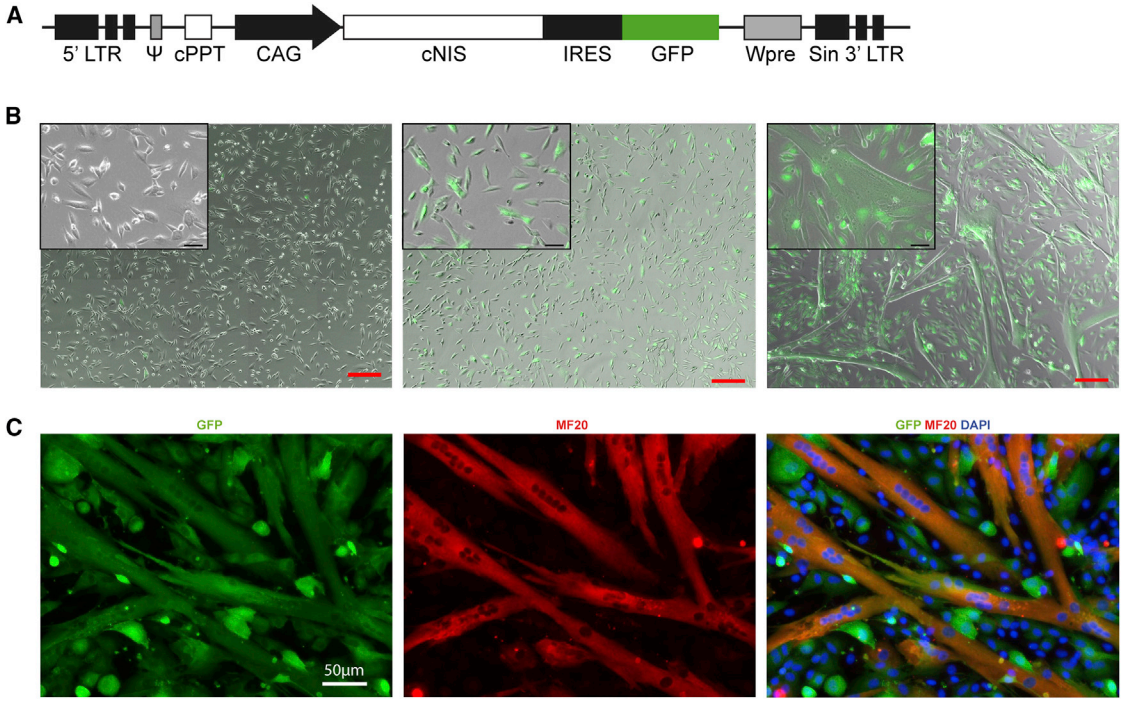

Figure 1. cNIS Expressing Canine Myoblasts Can Differentiate into Myotubes

(A) Graphical representation of the lentiviral vector pprl.sin.CAG-cNIS-IRES-GFP.Wpre used for the expression of cNIS and GFP cDNAs under the control of a CAG promoter. (B) Sorted cNIS-GFP$^-$ myoblasts (left) and cNIS-GFP$^+$ (middle and right) in proliferation media and for a week in differentiation media (right). Merge bright light and fluorescence microscopy images (GFP in green) scale bar (red), 200 µm. Insets: detail of zoomed cells, scale bar (black): 50 µm. (C) Expression of GFP and myosin heavy chain (MF20) in cNIS$^+$/GFP$^+$ canine myoblasts cultured under differentiation condition for 4 days.

single-photon emission computed tomography (SPECT) or PET imaging of the cells by indirect labeling, which has many advantages over direct labeling of cells, i.e., iron oxide, gold nanoparticles, radionuclides such ^{18}F-fluorodeoxyglucose or ^{111}In-oxine, or lanthanides such as gadolinium-DTPA (diethylenetriamine penta-acetic acid).[17–19] NIS is naturally expressed at the basal membrane of thyroid epithelial cells where it is responsible for the uptake of iodide, which is required for synthesis of thyroid hormones.[20] NIS is also expressed in the stomach, the salivary glands, and the testis.[21] By using compatible radioisotopes such as ^{123}I$^-$, ^{124}I$^-$, ^{131}I$^-$, tetra-fluoroborate (^{18}F) and $^{99\,m}$Tc-pertechnetate ($^{99\,m}$TcO$_4^-$), NIS overexpressing cells can be tracked *in vivo*.[22] The main advantages of a gene marker include the following: (1) it allows for the specific visualization of living cells because dead cells do not express the protein, (2) it allows for long-term monitoring by simple readministration of the tracker, and (3) it is compatible with biochemical and clinical evaluation tools.

NIS has been successfully used in preclinical studies as an imaging reporter for viral vector and cell-based therapies.[23,24] Indeed, it has been used to track cells such as the myogenic C2C12, myo-angiogenic MABs, cardiomyocytes derived from pluripotent stem cells,[25–27] or neural stem cells in the brain.[28] NIS was also used in clinical trials for tracking and treating myeloma using oncolytic viruses.[29] In large animal models, however, NIS was used to track cells in the cardiac muscle, but not in the skeletal muscle tissue.[30,31] The main objective of our study was to demonstrate the ability of NIS-based imaging to monitor intramuscularly injected myogenic cells *in vivo* in a large animal model and hence provide valuable information on the fate of these cells. We used canine NIS (cNIS) cDNA as a reporter gene for $^{99\,m}$TcO$_4^-$-based SPECT/CT imaging of canine myoblasts after intramuscular (IM) injection in healthy dogs. We observed that the expression of NIS did not interfere with the biology and differentiation capacity of myoblasts and allowed cell tracking *in vivo* for at least 1 month along with serial image acquisitions.

RESULTS

cNIS$^+$ Canine Myoblasts Maintain Their Myogenic Capacities

A lentiviral vector was generated for the long-term co-expression of cNIS and GFP proteins. The expression cassette containing a cNIS-IRES-GFP sequence was cloned under the control of a CAG promoter, providing the pprl.sin.CAG-cNIS-IRES-GFP.Wpre lentiviral vector (Figure 1A). Canine myoblasts at low passage (P2) were transduced with the lentiviral vector pprl.sin.CAG-cNIS-IRES-GFP.Wpre and after 2 more passages were sorted by FACS for their expression of GFP to obtain a pure cNIS-GFP $^+$ population (cNIS$^+$).

cNIS$^+$ and cNIS$^-$ myoblasts were grown in proliferative medium in parallel. When cultured for a week in differentiation medium,

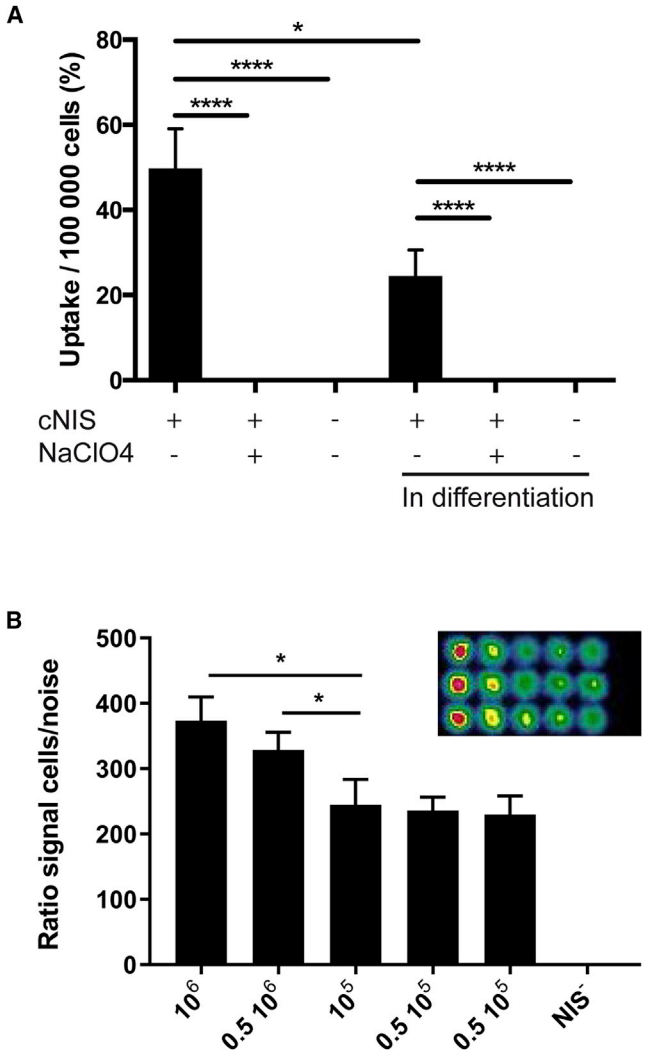

Figure 2. *In Vitro* Validation of Radiotracer Uptake by cNIS$^+$/GFP$^+$ Canine Myoblasts

(A) Measurement of $^{99\,m}TcO^-$ uptake efficiency by canine myoblasts sorted for GFP expression. The experiment was performed with cells under proliferation or after 5 days of differentiation. Sodium perchlorate ($NaClO_4$) was used for specific inhibition of NIS activity. NIS$^-$ myoblasts were used as negative control. Values were normalized to 1×10^5 cells. *p < 0.05 and ****p < 0.0001 of 3 independent experiments. (B) Imaging of *in vitro* cells. Different concentrations of cNIS myoblasts, 1×10^6, 0.5×10^6, 10^5, and twice 0.5×10^5 imaged after incubation with 185 kBq of $^{99\,m}TcO4^-$ imaged in a 12-well plate (upper right). Graphs represent ratio of cell uptake/surface area normalized by the background noise. Representative graph; each column represents three replicates. Statistical analysis performed with GraphPrism using one-way ANOVA test. *p < 0.05.

cNIS$^+$ myoblasts efficiently fused to form myotubes. From 4 days in culture with differentiation medium, cNIS$^+$ myoblasts displayed formation of myotubes (Figure 1B). This was confirmed by immunostaining using an antibody targeting the myosin heavy chain (Figure 1C). Immunostaining confirmed co-expression of the cNIS and the GFP, controlled by the same promoter, in transduced cells (Figure S1). A qPCR analysis of cNIS$^+$ myoblasts demonstrated that both transcripts (cNIS and GFP) were present. The maintenance of both transcripts was observed in cNIS$^+$ myoblasts through cell differentiation (Figure S2). Myotubes from cNIS$^+$ myoblasts also exhibited similar spontaneous contractions as not transduced cells (data not shown). We successfully obtained cells expressing cNIS using lentiviral vectors with a stable expression of the transgene to allow the long term tracking of cells *in vivo*.

In Vitro Uptake Efficiency of cNIS$^+$ Canine Myoblasts

Functionality of cNIS in transduced myoblasts was confirmed *in vitro* by measuring radionuclide uptake efficiency. Cells were incubated with $^{99\,m}TcO_4^-$ and the radionuclide uptake percentage was then measured and normalized to 1×10^5 cells (Figure 2A). cNIS$^+$ canine myoblasts cultured in growth medium showed an uptake radionuclide ratio of 49.76% (±10.75%) per 1×10^5 cells. In comparison, both wild-type (WT) myoblasts and cNIS$^+$ myoblasts incubated with sodium perchlorate, a NIS inhibitor, displayed 0.11% (±0.03%) and 0.13% (±0.04%) uptake, respectively. When cultured in differentiation medium, and after myotube formation, we observed 24.51% (±7.00%) of uptake by cNIS$^+$ myoblasts and 0.10% (±0.04%) and 0.12% (±0.03%) of uptake by WT myoblasts and cNIS$^+$ myoblasts incubated with sodium perchlorate, respectively. Different amounts of myoblasts going from 0.5×10^5 to 1×10^6 were plated and imaged for $^{99\,m}TcO_4^-$ uptake and all of them, including the lowest amount, were detected by the gamma camera. The signal was reduced in correlation with the decrease in number of cells. The uptake decrease was quantified using the ratio of counts per pixel, corrected for the noise (Figure 2B).

In order to confirm the capacity of the SPECT/CT to visualize cells in culture, cNIS$^+$ myoblasts were seeded and then imaged to assess their uptake of $^{99\,m}TcO_4^-$. After 1 h of incubation, rinsed cells and their removed supernatants were imaged separately. As expected, cNIS$^-$ cells showed no signal, with all of the radionuclide present in the supernatant; only cells expressing cNIS were detected (Figure S3).

Qualitative Imaging of cNIS$^+$ Canine Myoblasts after IM Injection in Dogs

In vivo experiments were detailed in Table 1. The first dog, Messmer, was injected in an autologous manner; IM injections were performed in the right *flexor carpi ulnaris* (rFCU), with 20×10^6 cNIS$^+$ myoblasts, in the right *triceps brachii* (rTB) 10×10^6 cNIS$^-$ and in the left *triceps brachii* (lTB) 10×10^6 cNIS$^+$ myoblasts. For all injected dogs, 629 MBq (22.2 MBq/kg) of $^{99\,m}TcO_4^-$ were injected 1 h before the onset of the SPECT/CT imaging examinations, which were performed at 4 h, 48 h, 7 days, and 30 days after cNIS$^+$ or cNIS$^-$ myoblast injections. We chose the $^{99\,m}TcO_4^-$ radionuclide because of its short half-life (6 h) and because of the positive results previously obtained *in vitro*. 4 h post cell injection and as expected, we observed a tropism of the tracer to the naturally NIS-expressing organs: stomach, thyroid, and salivary glands were strongly visible in the whole body planar acquisition. A weak signal was detected in the forearm corresponding to the rFCU muscle injected with 20×10^6 cNIS$^+$ myoblasts. Using

Table 1. Summary of *In Vivo* Experiments

Experiment	Dog	Age	Injected Muscle	Quantity of Injected Cells	Type of Graft	SPECT/CT Positive Signal			
1	Messmer	1 year, 7 months	rFCU	20×10^6 cNIS$^+$	autograft	X	X	X	
			lTB	10×10^6 cNIS$^+$		X	X		
			rTB	10×10^6 cNIS$^-$					
2	Messmer	1 year	Lvl	20×10^6 cNIS$^+$	autograft	X	X	X	X
			rTC	10×10^6 cNIS$^+$		X	X	X	
			rBF	3×10^6 cNIS$^+$		X			
			lTC	10×10^6 cNIS$^-$					
3	Jedi	2 year	rBF	3×10^6 cNIS$^+$	allograft	X	X		
			lTC	1×10^6 cNIS$^+$					
			rTB	5×10^5 cNIS$^+$					
			lBF	0.5×10^5 cNIS$^+$					
			lTB	3×10^6 cNIS$^-$					

rFCU, right *flexor carpi ulnaris*; lTB, left *triceps brachii*; rTB, right *triceps brachii*; lVL, left *vastus lateralis*; rTC, right *tibialis cranialis*; rBF, right *biceps femoris*; lTC, left *tibialis cranialis*. "X" corresponds to a radioactive signal.

SPECT/CT this site of injection was identified. The same result was obtained at 48 h with an additional signal in the lTB muscle injected with 10×10^6 cNIS$^+$ cells. At day 7, the imaging showed a signal from the rFCU muscle but a strong and diffuse signal was detected in the proximal part of the left forelimb, due to an edema, and preventing any reliable signal detection from injected cells in the lTB muscle. Both CT and MR imaging were performed and confirmed that a trauma of the shoulder joint caused an edema that progressively resolved in the following days, as well as the lameness. The imaging exam performed on day 30 did not show any signal within the injected muscles. Biopsies were performed after the last scan.

We demonstrated the visualization of 20 and 10 million injected cells expressing cNIS. Another experiment was done with 20 and 10 million and a lower quantity of cells, 3 million. Cells were injected in the same animal using injection sites distant from the other ones. Cells were injected as follows: 3×10^6 cNIS$^+$ myoblasts in the right *biceps femoris* (rBF), 10×10^6 cNIS$^+$ myoblasts in the right *tibialis cranialis* (rTC), 10×10^6 cNIS$^-$ myoblasts in the left *tibialis cranialis* (lTC), and finally 20×10^6 cNIS$^+$ myoblasts in the left *vastus lateralis* (lVL). Imaging was performed at the same time points: 4 h, 48 h, 7 days, and 30 days. From the 1st planar acquisition at 4 h after cell injection, apart from the endogenous signal of NIS-expressing organs, the higher quantity of cells was detected for a week in the hind limb probably corresponding to the lVL (20×10^6 cells) muscle (Figure 3A). This result was confirmed by the more precise axial SPECT/CT images where the spot was clearly visible and located in the lVL muscle at each imaging from 4 h to 30 days. Other symmetric non-specific uptake signals corresponding to bone/vasculature were visible in a symmetric pattern (Figure 3B). SPECT/CT axial images additionally showed a distinct focal signal at the other two injected sites with cNIS$^+$ cells and nothing at the cNIS$^-$ (lTC) site, as illustrated in Figure 4. The signal originating from the high doses of cells, 10 and 20×10^6 cells, was still detected again at the 3rd SPECT/CT scan performed at day 7. At day 30, (4th SPECT/CT), only the site injected with 20×10^6 cells showed a signal (Figure 4).

The third cell injection experiment was done in an immunosuppressed dog, Jedi, receiving allogeneic cells. To set the minimal threshold of cell detection, we injected a range of small cell numbers: from 0.5×10^5 cells into the lBF, 10^5 cells into the rTC, 5×10^5 cells into the rTB, 10^6 cells into the lTC, to 3×10^6 cells into the rBF, as well as 3×10^6 WT myoblasts from the same donor in the lTB, as a negative control. Sites of injection were chosen in remote regions in order to ensure that the signal could be distinguished from one site to another and from the physiologically NIS-expressing tissues. At 4 h post cell injection, a strong uptake was visualized in the organs known to physiologically express the NIS but no signal from any of the injection sites was visible. At 48 h post injection, the 2nd whole-body planar acquisition revealed a faint signal at the site of the 3×10^6 cNIS$^+$ myoblasts injection (Figure S4A, red arrow). Axial slice of the SPECT/CT acquisition revealed a clear signal coming from the injection site in the right BF muscle (Figure S4B). A strong signal was observed between thighs corresponding to the testes and to a lower extent to the tail. Lesser emitting spots were visible symmetrically in both thighs and were originating from the femur and the vasculature. No signal was observed from any of the other injection sites. Imaging at 7 and 30 days post injection of myoblasts showed no signal at any of the different injection sites but only in organs naturally expressing NIS. In view of these results, we established the amount of 3×10^6 of cNIS-expressing cells intramuscularly injected as a minimum threshold for *in vivo* detection with $^{99\,m}TcO_4^-$ SPECT/CT.

Quantification of SPECT/CT Signal

We quantified the signal detected by SPECT/CT imaging by delineating a region of interest (ROI) on axial slices around a radioactive site and placing the symmetrical ROI in the contralateral muscle. There was a concordance between signal and number of cells

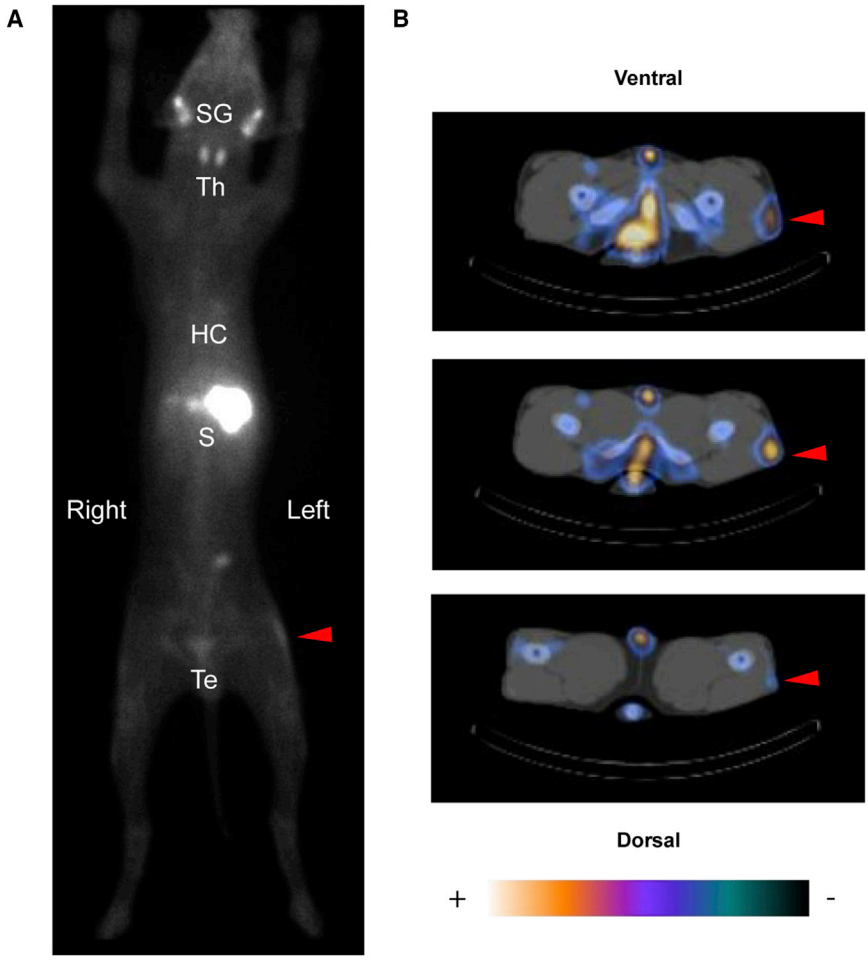

Figure 3. *In Vivo* Visualization of cNIS$^+$ Canine Cells
SPECT/CT visualization of 20 × 10^6 cNIS$^+$/GFP$^+$ cells (autologous, Messmer) at 7 days post injection. (A) Posterior view of the planar whole-body acquisition (1 h post $^{99\,m}TcO_4^-$ injection). Visualization of organs physiologically expressing NIS: salivary glands (SGs), thyroid (Th), stomach (S), and testes (Tes). There was also blood pool activity visible in the heart cavities (HCs). Linear increase uptake at the level of the left thigh (red arrowhead) indicating the 20 × 10^6 cNIS$^+$/GFP$^+$ cells injected in the left VL muscle. (B) Axial slices of the SPECT/CT acquisition at the level of the active uptake site, the upper slice corresponding to the more proximal image, and the lower one to the more distal. The region of increased uptake (indicated by a red arrowhead) was observed unilaterally and was anatomically compatible with the injection site, and so corresponds to NIS-mediated tracer uptake in the injected cells. No signal originating from the contralateral VL was detected. Linear uptake was visible in the blood vessels (blood pool) and the bones, probably due to bone marrow blood pool.

(repeatable among experiments): the higher the quantity of injected cells, the higher the signal detected. Figure 5 shows the evolution over time of the ratio of the ROI signal (counts) in the injected muscle divided by the counts in the contralateral muscle. At 48 h, a strong decrease of the signal was observed, followed by a less pronounced one until 7 days. The signal disappeared at 30 days except for the site of injection corresponding to 20 × 10^6 cNIS$^+$ myoblasts, which was still slightly active.

Histological Analysis of Injected Muscles

24 h after the last SPECT/CT acquisition, injected muscles were biopsied to assess the presence of cNIS-expressing myoblasts by immunofluorescence (IF) and by qPCR. 7 μm cryosections of all biopsied muscles were stained by IF against cNIS, which was detected in the rBF (3 × 10^6 cNIS$^+$ cells) and lVL (20 × 10^6 cNIS$^+$cells) muscles corresponding to the lowest and highest number of cells injected in Messmer dog. Of note, 1 month post cells injection, a clear spot was visible in the lVL by scintigraphy. As shown in Figure 6, cNIS protein was detected at the membrane of muscle fibers (lVL muscle) attesting a fusion of injected cNIS myoblasts and the correct sarcolemma localization of the cNIS protein. Quantitative evaluation on 5 random areas of biopsy cryosections showed 0.3% of cNIS$^+$ muscle fibers. Some infiltrates were also detected around the muscle fibers expressing cNIS. Further analysis demonstrated that these infiltrates were positive for CD4, CD8, and CD3 markers, but not CD11b (Figure S5).

RNA was isolated from biopsies' cryosections of Messmer dog, to assess the presence of cNIS transcript by qPCR. cNIS transcripts were detected at very low quantity corresponding to the latest cycles of the PCR (Figure S6), only in biopsies from lVL receiving 20 × 10^6 NIS$^+$ cells and from rBF receiving 3 × 10^6 cNIS$^+$ cells, which were already positive for NIS immunostaining and imaging.

DISCUSSION

In this study, transduced canine myoblasts expressing cNIS were consistently tracked by $^{99\,m}TcO_4^-$ scintigraphy for a month in dogs after IM administration. The tracking procedure was devoid of nonspecific signal within skeletal muscle allowing reliable tracking of myogenic cells in large animal models.

cNIS Reporter Gene Can Be Used to Track Myogenic Cells *In Vivo* without Interfering with Their Biology

Several clinical evaluation methods have been developed to study the functional effects of myogenic cell-based therapies. However, the lack of longitudinal non-invasive methodology for an *in vivo* cell-fate visualization still remains a major limitation. The NIS is naturally expressed in restricted well-known non-muscle organs and is therefore non-immunogenic, leading to an accurate monitoring of cell distribution in the entire body. This reporter gene has been already validated

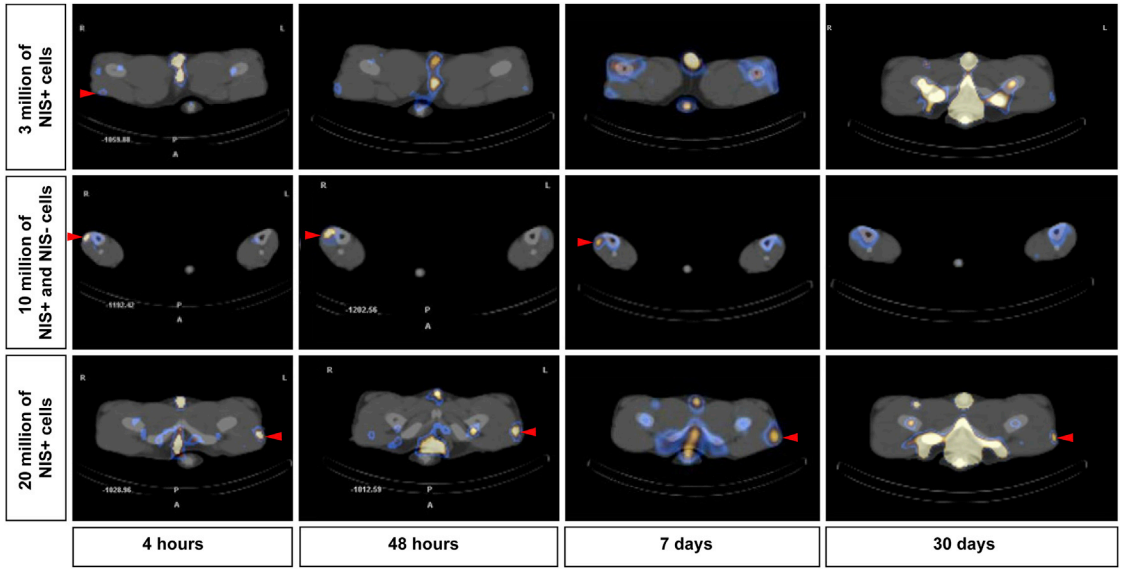

Figure 4. SPECT/CT Scans for cNIS$^+$ Cells Visualization

Axial slice of SPECT/CT images at different time points for three different amounts of IM injected (autologous) cells in a same experiment. In the first row, 3×10^6 of NIS$^+$ cells were injected into the rBF (red arrow) and no signal from the contralateral muscle was detected. Imaging was repeated at 48 h, 7 days, and 30 days, and no signal was visualized in the rBF muscle. Only symmetric slight spots corresponding to bone, vasculature, testis, or tail were visible. In the middle row, images corresponding to the TC muscles injected with 10×10^6 NIS$^+$ cells (right TC) and 10×10^6 of NIS$^-$ cells (left TC). Tracking of cells was possible for a week and only for the rTC injected with NIS$^+$ cells (red arrow) not detected in the less-sensitive planar acquisition. Symmetric spot in gray-blue corresponds to the tibias. In the last row of images, imaging of IVL muscle injected with 20×10^6 of NIS$^+$ cells tracked for a month (red arrow), with a clear focal signal at each image from 4 h to 30 days. No signal was detected in the contralateral muscle. In order to make visually detectable the low amount of radioactivity 30 days after injection, we adjusted the colormaps settings for the illustration to allow the visualization of NIS-expressing cells, but also leading to increased level of other structures (right column).

mainly in small animal models; studies in large animal models have focused on the cardiac muscle,[30,31] but not on the tracking of myogenic cells. Lee and colleagues[31] reported on AAV transduced canine stem cells (1×10^7) expressing the human NIS (hNIS) that were injected into the myocardium of healthy dogs; the peak of detection by SPECT/CT was seen at 48 h post administration with a follow up of 9 days. It is worth noting that the authors reported that hNIS expression had no impact on proliferation nor differentiation of the cells. Our study assesses the use of NIS to track transduced myogenic cells in large animal models. Here, we propose the use of cNIS as an imaging gene marker to monitor cells intramuscularly injected in the golden retriever dog, with the ultimate goal of transposing this tracking method into muscle cell therapy in GRMD dogs. We observed in our study that cNIS was biologically active both *in vitro* and *in vivo* and showed long-term expression in transduced cells avoiding loss of transgene expression suggested by Lee et al.[31] by using AAVs. Indeed, transduced cells were able to proliferate and to differentiate into myotubes *in vitro*, and to fuse with adult myofibers *in vivo*. A slight decrease in the uptake of cNIS was detected upon differentiation *in vitro* but regarding qPCR results, the small decrease in cNIS transcript expression was not statistically significant and direct imaging of differentiated cells showed a signal comparable to that of proliferating cells. The density of NIS at the membrane of myotubes may be reduced comparatively to that on the small surface of proliferating cells. An important point to consider for the correct NIS functionality is its accurate targeting to the plasma membrane and this was confirmed on injected muscle biopsies by IF. We used the CAG ubiquitous promoter, which is a strong driver of transgene expression in muscle and is not silenced through cell differentiation.[32–35] Even though differentiating myoblasts show *in vitro* reduced uptake efficiency compared to proliferating ones, the overall uptake was comparable to the values observed by others using mesenchymal stem cells or MABs.[19,26] and yielded satisfactory results allowing cell tracking *in vivo* for a month.

A Low Number of cNIS-Expressing Cells Can Be Detected in Injected Muscles for a Month

In vitro, as few as 0.5×10^5 cNIS$^+$ cells are clearly visualized by SPECT/CT. Higher doses were required for *in vivo* detection regardless of the source of the cells (allogeneic or autologous) that were administered, and regardless of whether the animals were immunosuppressed or immunocompetent; such treatments can modify cell biology and cell niche properties, but in the context of a proof-of principle study, we wanted to prevent a possible rejection not only due to the fact that the graft was allogenic, but also to the fact that cells were expressing the GFP. We found a relationship between the administered cell dose and the time the cells could be tracked. After *in vivo* administration of 3×10^6 NIS$^+$ cells, signal was detected up to 48 h (peak 4 h); however, higher doses, 20×10^6 NIS$^+$ cells, allowed effective detection for up to 1 month after administration. This is in

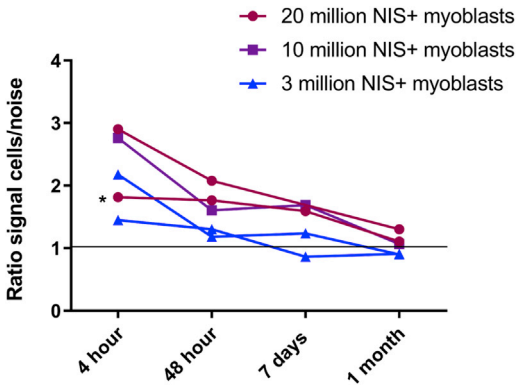

Figure 5. SPECT/CT Imaging Quantification

A region of interest (ROI) was delineated around each radioactive site and the symmetrical ROI in the contralateral muscle (Supplemental Materials and Methods). The ratio of signal in injected muscle to the signal in the contralateral muscle (either not injected or injected with NIS^- cells) is represented normalized by the area of the ROIs. Black asterisk corresponds to a delayed (+1 h) first imaging of cells after $^{99\ m}TcO_4^-$ injection due to a technical problem during the SPECT/CT acquisition. Grey horizontal line indicates the threshold of signal in the injected side over the contralateral side. Graphpad representation of two independent experiments of 3×10^6 and 20×10^6 $cNIS^+$ injected cells and one for 10×10^6 $cNIS^+$.

accordance with most of the studies using NIS imaging *in vivo* in mice, which managed to detect from 1 to 3×10^6 cells.[31,36] In large animals (pigs and dogs), 10^7 injected cells expressing NIS were detected after intracardiac injections.[31,37] In view of results using NIS-expressing cells tracked by SPECT/CT, the threshold of minimum detection by this technique may be much lower than the amount of injected cells and advantageous for this methodology. Indeed, IF analysis indicated that, within the tissue, a small number of cells (0.3%) fused with myofibers and expressing cNIS were still present at 1 month, probably due to massive cell death during and after cell injection. The presence of a SPECT/CT signal should therefore be due to a few thousands of injected cells, instead of a few million. Limitation of this study remains in the calculation of a precise number of NIS-expressing cells imaged and in the determination of detection sensitivity threshold not due to the methodology itself, but inherent to cell biology. The better sensitivity of detection in *in vitro* conditions could be explained by the fact that the *in vitro* setup does benefit from far better tracer accessibility and does not have any of the negative consequences of the *in vivo* injection, like massive cell death and radionuclide accessibility. A loss of injected myoblasts (up to 50%) within 48 h after the IM injection has been reported by others.[38–41] Consistently, we detected a decline of the signal of about 50% at 48 h (compared to the peak reached at 4 h) post cell injection as shown in Figure 5. This shows that the NIS-based cell tracking can be useful to reliably monitor cell survival *in vivo*, unlike other cell tracking methods such as the ^{111}In-oxine direct cell labeling, which we previously showed to be limited by cell-death-associated radioactivity release and non-specific signal on images (I.B., unpublished data). The massive cell death of injected myoblasts may have diverse origins. First, cell culture conditions may alter survival, migration, or fusion capacity of cells. Second, although the freshly isolated cells were mostly myogenic (60% expressed desmin and CD56 at passage 2), a progressive shift was observed in such a way that myogenic cells became minority at passage P9 (only 20% expressed desmin and CD56), suggesting cells may have lost stemness and undergone senescence. Third, in the present study, GFP protein unlike the canine NIS may have triggered an immunoreaction. Indeed, immunohistochemical analysis demonstrated that few cells were still alive and able to uptake radioactivity, but it detected numerous activated T cells surrounding the NIS-expressing cells *in vivo*. Moreover, previous experiments in our group showed prominent muscle infiltrates after IM injection of a plasmid expressing only GFP in an immunocompetent dog.

The combination of SPECT and CT allows precise localization and quantification of tracked-cells in a minimally invasive way by intermixing scintigraphy signals with anatomical imaging. The short half-life of $^{99\ m}TcO_4^-$ of only 6 h, contributes to a limited toxicity for cells, and the isolation of dogs receiving the radionuclide is diminished to 24 h instead of 3–4 weeks when using ^{111}In direct labeling of cells. The development of new radionuclides should even improve these parameters. Recently, tetra fluoroborate [^{18}F] was presented as a new candidate for NIS reporter imaging. This tracer, labeled with fluorine-18, which has a half-life of 109.8 min, showed very high uptake in NIS-expressing tissue in mice, macaques, and in the first clinical trials in healthy humans and benefits from the high sensitivity and spatial resolution of PET.[42] In order to improve the signal in the vicinity of natural NIS-expressing organs, others have suggested the use as pre-treatment of non-radioactive iodide (such as iodinated contrast) to reduce activity of naturally NIS-expressing tissues, in order to improve the detection of cells around these tissues (helpful in further systemic injections studies). This was not required in our study since NIS-expressing cells were intramuscularly injected in distant regions.[43]

To the best of our knowledge, there is no other work showing cNIS-expressing myoblasts injected in skeletal muscles of a large animal imaged by SPECT/CT for over a month. A remaining question is the possibility of detecting cells after intra-arterial delivery and dilution of $cNIS^+$ cells throughout a large territory. To precisely assess the threshold of cell detection, further experiments by intra-arterial delivery of cells able to migrate to damaged muscles, such as MABs,[10] must be tested. Finally, the use of viral vectors should be avoided to introduce the NIS transgene *in vitro* to avoid non-desired random genome insertions. In previous work of some co-authors, it has been shown the feasibility of stable genome edition using zinc-finger nucleases for imaging reporter genes, with PET detection.[44,45] In the near future, genome edition should be considered to establish a safe integration of NIS into the genome, through the use of CRISPR/Cas9 system.[46]

Conclusions

We proposed the use of NIS as a gene marker applied to muscle cell therapy; we have demonstrated some of the advantages of using NIS

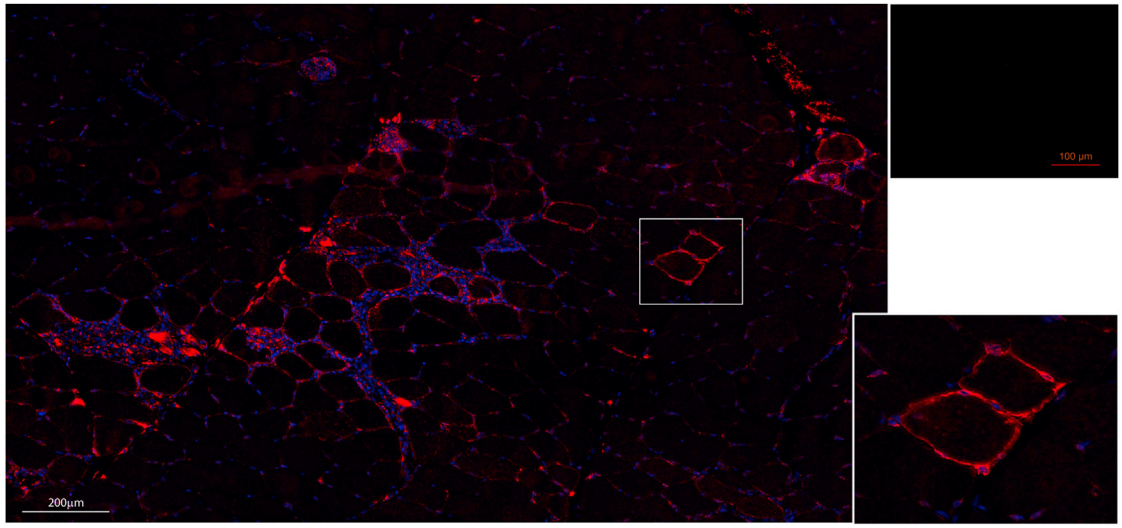

Figure 6. cNIS Expression in Muscle Fibers of Injected Muscles

Immunostaining against cNIS protein (in red) of a section of the left VL muscle injected with 20×10^6 $cNIS^+$ autologous myoblasts. The same muscle still presented a signal on the SPECT/CT images 1 month after myoblasts injection. Nuclei DAPI staining in blue showed some cell infiltrates surrounding NIS^+ cells. In the upper right image, a muscle injected with $cNIS^-$ cells. Inset shows detail of muscle fibers expressing cNIS at their membrane.

as a low invasive tracer for monitoring purposes in large animal models including disease models such as the GRMD dog for DMD. cNIS-expressing myoblasts maintained their proliferative and myogenic potential and displayed efficient radionuclide uptake *in vitro*. We have shown that a dose of 20×10^6 cells intramuscularly injected in dogs was detected for a month post injection. cNIS imaging could be used with different myogenic cell types (able to migrate such as MABS or induced pluripotent stem [iPS]-committed cells) to allow direct comparison of survival and biodistribution patterns, in the perspective of translation to clinical trials.

MATERIALS AND METHODS

Animals

All procedures were approved by the Ethical Committee of the ANSES, Ecole nationale vétérinaire d'Alfort, and UPEC (ComEth ANSES/EnvA/UPEC), under the approval number 20/12/12-20. Animals included in this study were healthy dogs housed in the facilities of the INSERM, IMRB U955-E10, Group 4-Neurobiology laboratory at Ecole nationale vétérinaire d'Alfort.

All *in vivo* experiments are summarized in Table 1.

Canine NIS cDNA Cloning

mRNA was extracted from a canine thyroid biopsy using Nucleospin RNA II Kit (Macherey-Nagel). cDNA synthesis was performed using the Maxima first strand cDNA synthesis kit (Thermo Fisher Scientific). Gateway system (Invitrogen) was used to amplify and clone cNIS cDNA in a pDONR223 plasmid. cNIS cDNA was transferred in a pCAGEN plasmid (Addgene #11160). The CAG promoter followed by cNIS cDNA was then introduced before the IRES sequence of a pprl.sin.IRES-GFP.Wpre lentiviral vector plasmid into the SpeI and SmaI cloning sites. Nucleobond Xtra Midi kit (Macherey-Nagel) was used for plasmid purification in nuclease-free conditions.

Canine Myoblasts Isolation and Culture

Myoblasts were isolated from dog BF biopsies. Muscle was minced in small fragments, rinsed with PBS + 2% FBS, and digested with type II collagenase (Worthington) for 1 h at 37°C followed by mechanic trituration using a 18G needle. Digestion product was filtrated with 100 µm and then 40 µm cell strainers. Cells were seeded in a flask with custom MCDB120-modified medium (HyClone) supplemented with 20% FBS (HyClone), 25 µg/mL gentamicin, 10 ng/mL basic fibroblast growth factor (bFGF) (Peprotech), and 10-6 M dexamethasone (Mylan) and cultured in a humidified incubator at 37°C with 20% O_2 and 5% CO_2. This custom made medium allows an enrichment of myoblasts cells through substitution of L-valine by D-valine inducing efficient inhibition of fibroblasts proliferation in benefit of myoblasts proliferation.[47] Cultured cells were immunophenotyped by the expression of desmin and CD56 as myogenic markers.[48] Myotube formation was induced by culturing myoblasts in DMEM supplemented with 2% horse serum and 1% penicillin/streptomycin for 3 to 7 days.

Lentiviral Vector Production, Myoblasts Transduction, and Sorting

HEK293T cells cultured in 10 cm Petri dishes were transfected ($CaPO_4$ transfection mediated by Cl_2Ca and HBS) with 4 µg vesicular stomatitis virus G protein (VSV-G) plasmid, 4 µg Gag-Pol plasmid, 4 µg Tat plasmid, and 10 µg pprl.sin.CAG-cNIS-IRES-GFP.Wpre plasmid. Viral vector particles-containing culture medium was harvested at 24 and 48 h post transfection. Viral vectors were concentrated by centrifugation with SW28 rotor (Beckman Coulter)

25,000 rpm, 120 min, 4°C, and resuspended in 90 μL of PBS. Titer was 5×10^6 transduction units/mL obtained by fluorescence-activated cell sorting (FACS) analysis. Myoblasts (at passage 3) seeded in a well of a 35 mm were transduced with 10 μL of viral vector suspension. After two passages (passage 4), transduced cells, mostly myoblasts, were sorted by FACS for their expression of GFP (30%) using an Influx v7 Sorter (BD FACS). Passages in cell factory plates were necessary for cell amplification (sorted at passage 4 and injected at passage P9).

In Vitro Radiotracer Uptake Experiment

$cNIS^-$ and $cNIS^+$ myoblasts were plated in quadruplicate in a 24-well plate for growth or differentiation. On the day of analysis, cells were incubated with $^{99\ m}TcO_4^-$ (185 kBq) in 200 μL DMEM for 1 h, specific NIS inhibition was obtained by addition of 10 μM sodium perchlorate ($NaClO_4$) in some wells. Medium was collected, along with the PBS used to rinse the cells. Cells were collected, counted with a NucleoCounter NC-100 (ChemoMetec), and lysed. Radioactivity of the cells and of the media was measured by a 2480 Wizard automatic gamma counter (PerkinElmer). Uptake values were corrected for each sample according to the number of cells. Data were presented as mean ± SEM. One-way ANOVA was performed for *in vitro* radiotracer uptake experiment. p values < 0.05 were considered statistically significant.

Intramuscular Injections

A 1-year-old male healthy golden retriever dog (Messmer) was injected intramuscularly with autologous myoblasts for two experiments (injected sites were placed far from others in order to avoid any interference). A 2-year-old male healthy golden retriever dog (Jedi) received allogeneic myoblast graft under an immunosuppressive treatment 3 weeks before graft and until the end of the experiment (association of prednisolone 2 mg/kg/d and cyclosporine A at a dose adjusted to maintain a trough cyclosporinemia between 300 and 400 ng/mL).

For the IM injection procedure, dogs were anaesthetized using an intravenous bolus of propofol (6.5 mg/kg) followed by the maintenance with inhaled isoflurane (2%–3% in 100% O_2). Continuous monitoring of electrocardiogram (ECG), pulsed saturation in dioxygen (SpO_2), end-tidal CO_2 ($ETCO_2$), and rectal temperature were set up. Each selected muscle was exposed after a cutaneous incision and injections were performed as follows: a small group of fascicles was identified and an injection site was delineated using two non-absorbable sutures (prolene 4-0) tied apart. The cells were suspended in 500 μL of PBS containing 5% of serum from the recipient dog, and injected using a 100 μL Hamilton syringe mounted with a 30G needle. Multisite injections were repeated along the delineated site. The peroperative analgesia was ensured using intravenously administered morphine (0.1 mg/kg).

SPECT/CT Imaging

Dogs received an intravenous injection of 629 MBq (22.2 MBq/kg) of $^{99\ m}TcO_4^-$ (left distal cephalic vein) and were anaesthetized as described above. Scintigraphic static acquisitions were performed on the same day as the cell injections (4 h after injection), at 48 h, 7 days, and 30 days after using an Infinia II 3/8 Hawkeye Hybrid NM/CT (GE) with low energy high-resolution collimators and energy window peaked at 140 keV.

The same imaging protocol was applied for each dog at each acquisition: first, at 45 min after $^{99\ m}TcO_4^-$ injection, a whole body planar acquisition (20 min) was performed, using a 256 × 256 matrix and a pixel size of 2.21 × 2.21 mm. Then a SPECT/CT sequence lasting 30 min was performed at the level of the thoracic or pelvic limbs, depending on the injection sites. A SPECT sequence lasting 20 min was performed using a 128 × 128 matrix, a pixel size of 4.42 × 4.42 mm, and acquisitions of images at 30 different positions of the dual head camera, over a 360° rotation, each projection being acquired during 40 s. A CT lasting 10 min was then performed, at 140 kV, 2.5 mA, and with a slice thickness of 10 mm. The images were reconstructed in the Xeleris (GE) workstation.

For cell dishes imaging, the plates were positioned directly on one of the collimators, a 256 × 256 matrix was used, and the size of pixels was 2.21 × 2.21. The static acquisition lasted 5 min.

Image Analysis

The images were analyzed in the Xeleris (GE) workstation. The SPECT/CT images were observed in the three different axes to identify putative injection sites based on signal presence and compatibility with anatomical location. The quantitative analysis was performed on axial views by drawing a ROI around the identified signal spot, over the three consecutive slices on which the signal was the strongest visually. A symmetric ROI was set on the contralateral limb. The ratio of the injected side signal and the contralateral side signal (counts/pixel) was used for the analysis of the results (Supplemental Materials and Methods). The slice exhibiting the highest signal ratio was kept for the analysis, assuming that it should be the closest to the actual injection site.

For cell culture imaging analysis, ROIs were drawn around the scintigraphy images of the culture wells and the values were corrected for background signal.

Immunostaining

7 μm slices cryostat sections were fixed with acetone/methanol 10 min at −20°C. Nonspecific sites were blocked with 0.1% Tween 20 + 3% BSA in Tris-buffered saline (TBS) 1 h, room temperature (RT). Tissue slices were stained with the mouse anti-NIS Ab clone 2-2 (Millipore) in TBS + 0.1% Tween 20 + 3% BSA (overnight, 4°C), then with anti-mouse Alexa Fluor 488 in TBS + 0.1% Tween 20 + 3% BSA (1 h, RT). Nuclear staining was performed with DAPI (4',6-diamidino-2-phénylindole), Sigma-Aldrich (300 nM).

Differentiated myoblasts in culture were fixed with 4% paraformaldehyde in PBS (10 min, RT) and permeabilized with 0.5% Triton X-100 in PBS + 2% BSA (45 min, RT). Cells were incubated overnight with mouse anti-MF20 Ab (1/4, produced in house) and rabbit anti-GFP

Ab (1/300) in PBS + 2% BSA and then with 1 anti-mouse Alexa Fluor 647 Ab (Jackson ImmunoResearch, 1/500) and anti-rabbit Ab Alexa Fluor 488 (Jackson ImmunoResearch, 1/500) in PBS + 2% BSA. Nuclear staining was performed with DAPI.

RNA Extraction

RNA was extracted from transduced cells and from frozen muscles, using the Nucleospin RNA Plus Kit (Macherey-Nagel). Concentrations and purity of RNAs were determined using a NanoDrop (Thermo Fisher Scientific). cDNA synthesis was performed using the Maxima first strand cDNA synthesis kit (Thermo Fisher Scientific). Reverse transcriptase minus controls (without reverse transcriptase) was carried out for each retro-transcription.

Quantitative Real-Time PCR

Analysis of NIS-expressing cells by qPCR was carried out using 1 μg of total RNA. After the retro transcription to cDNA, cDNA was used in triplicates for each sample and pair of primers. Power SYBR green master mix (Thermo Fisher Scientific) was used as reagent in a Light Cycler p96 (Roche). The amplification protocol: pre-incubation at 95°C for 5 min and then 45 cycles at 95°C for 15 s, 59°C for 20 s, and 72°C for 20 s. At the end, a cycle of high resolution melting was added. The delta-delta-Ct algorithm (DDCt) method was applied to determine the expression level of target genes relative to the RPS19 (housekeeping gene), whose expression does not vary between samples, and referred to cells non-expressing NIS.

SUPPLEMENTAL INFORMATION

Supplemental Information can be found online at https://doi.org/10.1016/j.omtm.2019.12.011.

AUTHOR CONTRIBUTIONS

I.P., D.M., J.-L.T., C.M.D., J.-T.V., M.S., I.B., and S.B. designed the experiments. S.B. provided funding. I.P., D.M., B.H., P.d.F., N.B.-G., and I.B. performed the experiments. I.P., D.M., and I.B. analyzed the data. I.P., D.M., I.B., J.-T.V., and S.B. wrote the manuscript. All authors read and approved the final manuscript.

CONFLICTS OF INTEREST

The authors declare no competing interests.

ACKNOWLEDGMENTS

The authors acknowledge financial support of their work by Agence Nationale de la Recherche (Laboratoire d'Excellence Revive, ANR-10-LABX-73) and Association Française contre les Myopathies (AFM), France (grant n°18073). We thank Laurent Tiret and Bernard Klonjkowski for the provision of their laboratories for molecular biology experiments and lentiviral production, respectively. We thank Hélène Vandenberghe for cNIS qPCR primers and Angeles Escarti Nebot for helping with manuscript revision. We thank Anne Hulin and her team in the Laboratoire de Pharmacologie-Toxicologie in the Hôpital Henri Mondor, Créteil, for the cyclosporinemia assays and for their invaluable support. We thank Xavier Cauchois, Quentin Le Roux, and Romain François for technical assistance on *in vivo* experiments and the whole teams of BNMS, Group 4 in the EnvA, and of MICEN Vet, Créteil, for taking very good care of the dogs included in this study.

REFERENCES

1. Tedesco, F.S., and Cossu, G. (2012). Stem cell therapies for muscle disorders. Curr. Opin. Neurol. *25*, 597–603.
2. Iyer, P.S., Mavoungou, L.O., Ronzoni, F., Zemla, J., Schmid-Siegert, E., Antonini, S., Neff, L.A., Dorchies, O.M., Jaconi, M., Lekka, M., et al. (2018). Autologous Cell Therapy Approach for Duchenne Muscular Dystrophy using PiggyBac Transposons and Mesoangioblasts. Mol. Ther. *26*, 1093–1108.
3. Hoffman, E.P., Brown, R.H., Jr., and Kunkel, L.M. (1987). Dystrophin: the protein product of the Duchenne muscular dystrophy locus. Cell *51*, 919–928.
4. Emery, A.E. (1993). Duchenne muscular dystrophy–Meryon's disease. Neuromuscul. Disord. *3*, 263–266.
5. Emery, A.E. (2002). The muscular dystrophies. Lancet *359*, 687–695.
6. Kieny, P., Chollet, S., Delalande, P., Le Fort, M., Magot, A., Pereon, Y., and Perrouin Verbe, B. (2013). Evolution of life expectancy of patients with Duchenne muscular dystrophy at AFM Yolaine de Kepper centre between 1981 and 2011. Ann. Phys. Rehabil. Med. *56*, 443–454.
7. Mah, J.K. (2016). Current and emerging treatment strategies for Duchenne muscular dystrophy. Neuropsychiatr. Dis. Treat. *12*, 1795–1807.
8. Barthélémy, F., and Wein, N. (2018). Personalized gene and cell therapy for Duchenne Muscular Dystrophy. Neuromuscul. Disord. *28*, 803–824.
9. Shieh, P.B. (2018). Emerging Strategies in the Treatment of Duchenne Muscular Dystrophy. Neurotherapeutics *15*, 840–848.
10. Sampaolesi, M., Torrente, Y., Innocenzi, A., Tonlorenzi, R., D'Antona, G., Pellegrino, M.A., Barresi, R., Bresolin, N., De Angelis, M.G., Campbell, K.P., et al. (2003). Cell therapy of alpha-sarcoglycan null dystrophic mice through intra-arterial delivery of mesoangioblasts. Science *301*, 487–492.
11. Mitchell, K.J., Pannérec, A., Cadot, B., Parlakian, A., Besson, V., Gomes, E.R., Marazzi, G., and Sassoon, D.A. (2010). Identification and characterization of a non-satellite cell muscle resident progenitor during postnatal development. Nat. Cell Biol. *12*, 257–266.
12. Rouger, K., Larcher, T., Dubreil, L., Deschamps, J.Y., Le Guiner, C., Jouvion, G., Delorme, B., Lieubeau, B., Carlus, M., Fornasari, B., et al. (2011). Systemic delivery of allogenic muscle stem cells induces long-term muscle repair and clinical efficacy in duchenne muscular dystrophy dogs. Am. J. Pathol. *179*, 2501–2518.
13. Tedesco, F.S., Dellavalle, A., Diaz-Manera, J., Messina, G., and Cossu, G. (2010). Repairing skeletal muscle: regenerative potential of skeletal muscle stem cells. J. Clin. Invest. *120*, 11–19.
14. Kornegay, J.N. (2017). The golden retriever model of Duchenne muscular dystrophy. Skelet. Muscle *7*, 9.
15. Sampaolesi, M., Blot, S., D'Antona, G., Granger, N., Tonlorenzi, R., Innocenzi, A., Mognol, P., Thibaud, J.L., Galvez, B.G., Barthélémy, I., et al. (2006). Mesoangioblast stem cells ameliorate muscle function in dystrophic dogs. Nature *444*, 574–579.
16. Cossu, G., Previtali, S.C., Napolitano, S., Cicalese, M.P., Tedesco, F.S., Nicastro, F., Noviello, M., Roostalu, U., Natali Sora, M.G., Scarlato, M., et al. (2015). Intra-arterial transplantation of HLA-matched donor mesoangioblasts in Duchenne muscular dystrophy. EMBO Mol. Med. *7*, 1513–1528.
17. Kraitchman, D.L., Tatsumi, M., Gilson, W.D., Ishimori, T., Kedziorek, D., Walczak, P., Segars, W.P., Chen, H.H., Fritzges, D., Izbudak, I., et al. (2005). Dynamic imaging of allogeneic mesenchymal stem cells trafficking to myocardial infarction. Circulation *112*, 1451–1461.
18. Kang, W.J., Kang, H.J., Kim, H.S., Chung, J.K., Lee, M.C., and Lee, D.S. (2006). Tissue distribution of 18F-FDG-labeled peripheral hematopoietic stem cells after intracoronary administration in patients with myocardial infarction. J. Nucl. Med. *47*, 1295–1301.
19. Wolfs, E., Holvoet, B., Gijsbers, R., Casteels, C., Roberts, S.J., Struys, T., Maris, M., Ibrahimi, A., Debyser, Z., Van Laere, K., et al. (2014). Optimization of multimodal

imaging of mesenchymal stem cells using the human sodium iodide symporter for PET and Cerenkov luminescence imaging. PLoS ONE *9*, e94833.

20. Portulano, C., Paroder-Belenitsky, M., and Carrasco, N. (2014). The Na+/I- symporter (NIS): mechanism and medical impact. Endocr. Rev. *35*, 106–149.
21. Dohán, O., De la Vieja, A., Paroder, V., Riedel, C., Artani, M., Reed, M., Ginter, C.S., and Carrasco, N. (2003). The sodium/iodide Symporter (NIS): characterization, regulation, and medical significance. Endocr. Rev. *24*, 48–77.
22. Ahn, B.C. (2012). Sodium iodide symporter for nuclear molecular imaging and gene therapy: from bedside to bench and back. Theranostics *2*, 392–402.
23. Terrovitis, J., Kwok, K.F., Lautamäki, R., Engles, J.M., Barth, A.S., Kizana, E., Miake, J., Leppo, M.K., Fox, J., Seidel, J., et al. (2008). Ectopic expression of the sodium-iodide symporter enables imaging of transplanted cardiac stem cells in vivo by single-photon emission computed tomography or positron emission tomography. J. Am. Coll. Cardiol. *52*, 1652–1660.
24. Penheiter, A.R., Russell, S.J., and Carlson, S.K. (2012). The sodium iodide symporter (NIS) as an imaging reporter for gene, viral, and cell-based therapies. Curr. Gene Ther. *12*, 33–47.
25. Bouchentouf, M., Benabdallah, B.F., Dumont, M., Rousseau, J., Jobin, L., and Tremblay, J.P. (2005). Real-time imaging of myoblast transplantation using the human sodium iodide symporter. Biotechniques *38*, 937–942.
26. Holvoet, B., Quattrocelli, M., Belderbos, S., Pollaris, L., Wolfs, E., Gheysens, O., Gijsbers, R., Vanoirbeek, J., Verfaillie, C.M., Sampaolesi, M., and Deroose, C.M. (2015). Sodium Iodide Symporter PET and BLI Noninvasively Reveal Mesoangioblast Survival in Dystrophic Mice. Stem Cell Reports *5*, 1183–1195.
27. Giacomazzi, G., Holvoet, B., Trenson, S., Caluwé, E., Kravic, B., Grosemans, H., Cortés-Calabuig, Á., Deroose, C.M., Huylebroeck, D., Hashemolhosseini, S., et al. (2017). MicroRNAs promote skeletal muscle differentiation of mesodermal iPSC-derived progenitors. Nat. Commun. *8*, 1249.
28. Micci, M.A., Boone, D.R., Parsley, M.A., Wei, J., Patrikeev, I., Motamedi, M., and Hellmich, H.L. (2015). Development of a novel imaging system for cell therapy in the brain. Stem Cell Res. Ther. *6*, 131.
29. Dispenzieri, A., Tong, C., LaPlant, B., Lacy, M.Q., Laumann, K., Dingli, D., Zhou, Y., Federspiel, M.J., Gertz, M.A., Hayman, S., et al. (2017). Phase I trial of systemic administration of Edmonston strain of measles virus genetically engineered to express the sodium iodide symporter in patients with recurrent or refractory multiple myeloma. Leukemia *31*, 2791–2798.
30. Templin, C., Zweigerdt, R., Schwanke, K., Olmer, R., Ghadri, J.R., Emmert, M.Y., Müller, E., Küest, S.M., Cohrs, S., Schibli, R., et al. (2012). Transplantation and tracking of human-induced pluripotent stem cells in a pig model of myocardial infarction: assessment of cell survival, engraftment, and distribution by hybrid single photon emission computed tomography/computed tomography of sodium iodide symporter transgene expression. Circulation *126*, 430–439.
31. Lee, A.R., Woo, S.K., Kang, S.K., Lee, S.Y., Lee, M.Y., Park, N.W., Song, S.H., Lee, S.Y., Nahm, S.S., Yu, J.E., et al. (2015). Adenovirus-mediated expression of human sodium-iodide symporter gene permits in vivo tracking of adipose tissue-derived stem cells in a canine myocardial infarction model. Nucl. Med. Biol. *42*, 621–629.
32. Niwa, H., Yamamura, K., and Miyazaki, J. (1991). Efficient selection for high-expression transfectants with a novel eukaryotic vector. Gene *108*, 193–199.
33. Alexopoulou, A.N., Couchman, J.R., and Whiteford, J.R. (2008). The CMV early enhancer/chicken beta actin (CAG) promoter can be used to drive transgene expression during the differentiation of murine embryonic stem cells into vascular progenitors. BMC Cell Biol. *9*, 2.
34. Evans, V., Foster, H., Graham, I.R., Foster, K., Athanasopoulos, T., Simons, J.P., Dickson, G., and Owen, J.S. (2008). Human apolipoprotein E expression from mouse skeletal muscle by electrotransfer of nonviral DNA (plasmid) and pseudotyped recombinant adeno-associated virus (AAV2/7). Hum. Gene Ther. *19*, 569–578.
35. Powell, S.K., Rivera-Soto, R., and Gray, S.J. (2015). Viral expression cassette elements to enhance transgene target specificity and expression in gene therapy. Discov. Med. *19*, 49–57.
36. Pan, Y., Liu, S., Wu, H., Lv, J., Xu, X., and Zhang, Y. (2013). Baculovirus as an ideal radionuclide reporter gene vector: a new strategy for monitoring the fate of human stem cells in vivo. PLoS ONE *8*, e61305.
37. Hickey, R.D., Mao, S.A., Glorioso, J., Elgilani, F., Amiot, B., Chen, H., Rinaldo, P., Marler, R., Jiang, H., DeGrado, T.R., et al. (2016). Curative ex vivo liver-directed gene therapy in a pig model of hereditary tyrosinemia type 1. Sci. Transl. Med. *8*, 349ra99.
38. Fan, Y., Maley, M., Beilharz, M., and Grounds, M. (1996). Rapid death of injected myoblasts in myoblast transfer therapy. Muscle Nerve *19*, 853–860.
39. Smythe, G.M., Hodgetts, S.I., and Grounds, M.D. (2000). Immunobiology and the future of myoblast transfer therapy. Mol. Ther. *1*, 304–313.
40. Skuk, D., Caron, N.J., Goulet, M., Roy, B., and Tremblay, J.P. (2003). Resetting the problem of cell death following muscle-derived cell transplantation: detection, dynamics and mechanisms. J. Neuropathol. Exp. Neurol. *62*, 951–967.
41. Skuk, D., and Tremblay, J.P. (2017). Cell Therapy in Myology: Dynamics of Muscle Precursor Cell Death after Intramuscular Administration in Non-human Primates. Mol. Ther. Methods Clin. Dev. *5*, 232–240.
42. Jiang, H., and DeGrado, T.R. (2018). [^{18}F]Tetrafluoroborate ([^{18}F]TFB) and its analogs for PET imaging of the sodium/iodide symporter. Theranostics *8*, 3918–3931.
43. Vassaux, G., Zwarthoed, C., Signetti, L., Guglielmi, J., Compin, C., Guigonis, J.M., Juhel, T., Humbert, O., Benisvy, D., Pourcher, T., and Cambien, B. (2018). Iodinated Contrast Agents Perturb Iodide Uptake by the Thyroid Independently of Free Iodide. J. Nucl. Med. *59*, 121–126.
44. Wolfs, E., Holvoet, B., Ordovas, L., Breuls, N., Helsen, N., Schönberger, M., Raitano, S., Struys, T., Vanbilloen, B., Casteels, C., et al. (2017). Molecular Imaging of Human Embryonic Stem Cells Stably Expressing Human PET Reporter Genes After Zinc Finger Nuclease-Mediated Genome Editing. J. Nucl. Med. *58*, 1659–1665.
45. Neyrinck, K., Breuls, N., Holvoet, B., Oosterlinck, W., Wolfs, E., Vanbilloen, H., Gheysens, O., Duelen, R., Gsell, W., Lambrichts, I., et al. (2018). The human somatostatin receptor type 2 as an imaging and suicide reporter gene for pluripotent stem cell-derived therapy of myocardial infarction. Theranostics *8*, 2799–2813.
46. Mali, P., Yang, L., Esvelt, K.M., Aach, J., Guell, M., DiCarlo, J.E., Norville, J.E., and Church, G.M. (2013). RNA-guided human genome engineering via Cas9. Science *339*, 823–826.
47. Vilquin, J.T., Marolleau, J.P., Sacconi, S., Garcin, I., Lacassagne, M.N., Robert, I., Ternaux, B., Bouazza, B., Larghero, J., and Desnuelle, C. (2005). Normal growth and regenerating ability of myoblasts from unaffected muscles of facioscapulohumeral muscular dystrophy patients. Gene Ther. *12*, 1651–1662.
48. Stewart, J.D., Masi, T.L., Cumming, A.E., Molnar, G.M., Wentworth, B.M., Sampath, K., McPherson, J.M., and Yaeger, P.C. (2003). Characterization of proliferating human skeletal muscle-derived cells in vitro: differential modulation of myoblast markers by TGF-beta2. J. Cell. Physiol. *196*, 70–78.